1-1-1994

Spectroscopy And Green Up-Conversion Laser-Emission Of Er(3+)-Doped Crystals At Room-Temperature

T. Danger

J. Koetke

R. Brede

E. Heumann

G. Huber

See next page for additional authors

Spectroscopy and green upconversion laser emission of Er^{3+}-doped crystals at room temperature

Cite as: Journal of Applied Physics **76**, 1413 (1994); https://doi.org/10.1063/1.357745
Submitted: 17 February 1994 . Accepted: 19 April 1994 . Published Online: 17 August 1998

T. Danger, J. Koetke, R. Brede, E. Heumann, G. Huber, and B. H. T. Chai

Spectroscopy and green upconversion laser emission of Er^{3+}-doped crystals at room temperature

T. Danger, J. Koetke, R. Brede, E. Heumann, and G. Huber
Institut für Laser-Physik, Universität Hamburg, Jungiusstrasse 11, D-20355 Hamburg, Germany

B. H. T. Chai
Center for Research in Electro Optics and Lasers (CREOL), University of Central Florida, Orlando, Florida 32826

(Received 17 February 1994; accepted for publication 19 April 1994)

The spectroscopic parameters of Er^{3+}-doped crystals were determined with regard to the upconversion laser parameters of the green transition ${}^4S_{3/2} \rightarrow {}^4I_{15/2}$. The influence of excited-state absorption on this laser channel was determined. Furthermore, upconversion pump mechanisms using ground-state and excited-state absorption around 810 and 970 nm were investigated by direct measurements of excited-state absorption. The spectroscopic results confirm the pulsed room-temperature laser experiments on the ${}^4S_{3/2} \rightarrow {}^4I_{15/2}$ transition. The lasers based on Er:$LiYF_4$, Er:$Y_3Al_5O_{12}$, and Er:$Lu_3Al_5O_{12}$ were directly excited into the upper laser level by an excimer laser pumped dye laser in the blue spectral range. In Er:$LiYF_4$, Er:KYF_4, and Er:$Y_3Al_5O_{12}$, laser action was achieved with two-step upconversion pumping by a Ti:sapphire laser and a krypton ion laser. In the case of the fluorides, the additional pumping with the krypton ion laser was not necessary. The laser emission wavelengths were 551 nm for Er:$LiYF_4$, 561 nm for Er:$Y_3Al_5O_{12}$ and Er:$Lu_3Al_5O_{12}$, and 562 nm for Er:KYF_4. In addition, green quasi-cw laser emission of Er:$LiYF_4$ pumped with an argon-ion laser was realized at room temperature.

I. INTRODUCTION

The interest in developing compact blue and green laser sources for data storage and display applications was increased by promising investigations on wide gap semiconductor diode lasers,[1,2] harmonic generation by phase matching in nonlinear crystals[3] or quasi-phase matching in optical fibers and other waveguides,[4] and upconversion lasers in crystals[5] and fibers.[6,7] While in the case of wide gap semiconductor diodes room-temperature laser operation is difficult because of growth and doping problems, harmonic generation is a well-known technique. Using diode pumped Nd lasers, conversion efficiencies of about 20% are achieved by internal frequency doubling.[8,9] However, accurate phase matching requires critical alignment of the nonlinear crystals.

Lasers which emit at higher frequencies than the pump light usually are called upconversion lasers. In these lasers the active ion is usually excited by internal upconversion of near-infrared or red light via multistep photon excitation or cooperative energy transfer and emits anti-Stokes visible light. In initial upconversion laser research, cryogenic temperatures were required and the observed efficiencies were very low. The advent and rapid improvement of high power laser diodes in the red and near-infrared spectral ranges have caused new interest in the development of upconversion lasers. The output wavelength of laser diodes can be tuned to match the absorption lines of the active laser ion, resulting in a substantial fraction of ions excited into higher energy levels, thus enhancing the upconversion process. Visible upconversion lasing at room temperature has already been demonstrated in Tm-doped crystals[10,11] and in various rare-earth doped fluorozirconate fibers.[7,12]

Er^{3+} is also an attractive laser ion with several optical transitions in the visible spectral range. Due to its complex energy-level scheme (see Fig. 1) with some metastable excited states, Er^{3+} gives rise to multiple cooperative energy transfer and excited-state absorption processes, which can be utilized for upconversion pumping. Green laser emission on the transition ${}^4S_{3/2} \rightarrow {}^4I_{15/2}$ of Er^{3+} has already been realized both with short-wavelength excitation[14] and with upconversion pumping.[15,16] Continuous-wave upconversion lasing of Er^{3+}-doped $LiYF_4$ (YLF) has also been reported.[17–19] However, cryogenic temperatures were required for these lasers, so their applications were limited. The first green room-temperature laser emission of Er^{3+} was published in 1993 with direct excitation in the blue spectral range.[20] Recently, green upconversion laser emission of Er^{3+}-doped crystals at room temperature was realized in the pulsed[21] and in the cw mode.[22]

In this paper, the spectroscopic parameters of the green transition ${}^4S_{3/2} \rightarrow {}^4I_{15/2}$ in Er-doped $Y_3Al_5O_{12}$ (YAG), YLF, and KYF_4 (KYF) are presented. The influence of excited-state absorption on this laser channel was investigated. Stimulated emission spectra were compared with the laser parameters. Ground-state absorption and direct excited-state absorption measurements around 810 and 970 nm wavelength were performed in order to investigate two specific pumping schemes for a green upconversion Er^{3+} laser at room temperature. The laser data of the Er:YLF laser at 551 nm were compared for pumping with a pulsed Ti:sapphire laser around 810 and 970 nm wavelength, respectively. In principle, the Ti:sapphire laser could be replaced by laser diodes for a compact all-solid-state device.

 0021-8979/94/76(3)/1413/10/$6.00

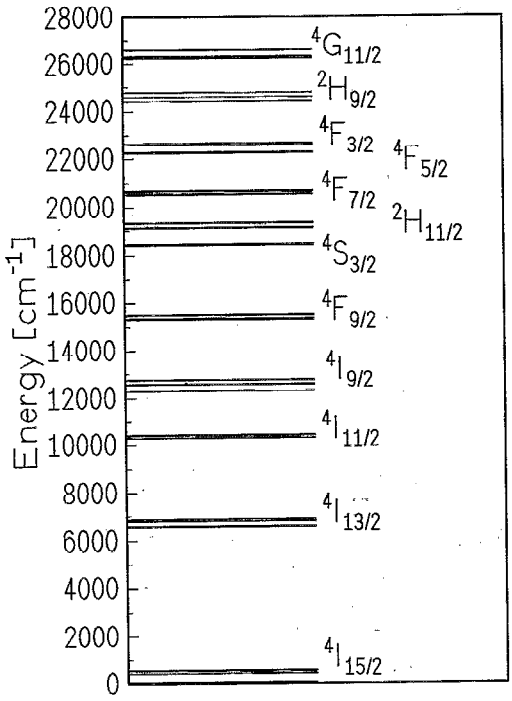

FIG. 1. Energy-level scheme for Er:YAG at 77 K (after Ref. 13).

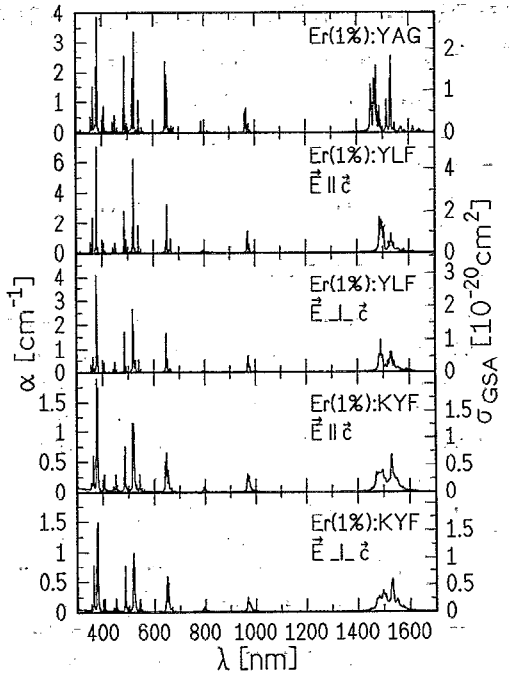

FIG. 2. Ground-state absorption spectrum of Er-doped YAG, YLF, and KYF.

II. SPECTROSCOPY

In this section the basic spectroscopic properties of Er-doped YAG, YLF, and KYF are presented, with the main emphasis on excited-state absorption (ESA). Absorption and fluorescence spectra are briefly reviewed.

With regard to the laser experiments, ESA plays an important role in at least two ways. Firstly, parasitic ESA at the laser wavelength may reduce the efficiency of a laser transition or even prevent the laser from oscillating at all. Such an effect has been supposed earlier in the case of the green laser transition $^4S_{3/2} \rightarrow {}^4I_{15/2}$ in Er^{3+}.[14,23] Secondly, upconversion lasers may be efficiently pumped by a two-step process including one ground-state absorption and one ESA process (see Sec. III C). Therefore, for a systematic selection of pump wavelengths and polarizations, ESA spectra are required.

A. Ground-state absorption

The ground-state absorption spectra of the investigated crystals were measured with a Cary 17 D photospectrometer. The effective ground-state absorption cross sections σ_{GSA} can be determined from the absorption coefficients α and the concentration n of the active ions via $\sigma_{GSA}=\alpha/n$. For the atomic cross sections, the population densities of the different Stark levels due to the Boltzmann statistics have to be taken into account. The large number of energy levels of the Er^{3+} ion yields several absorption bands. In Fig. 2 the ground-state absorption spectra of different Er-doped crystals are shown. The percentage of doping in Fig. 2 is given with respect to the lattice site, in this case the Y site. It was assumed that the Er^{3+} doping level in the crystal is the same as in the melt.

YAG is a cubic host lattice. Therefore, the spectroscopic parameters of Er:YAG are isotropic. The absorption bands at around 500 nm can be used for argon-ion laser pumping. Near 800 and 970 nm, where powerful laser diodes are available, there are absorption bands as well as ESA transitions (see Sec. II C). Consequently, these spectral regions are interesting with regard to upconversion lasers. In the case of Er:YLF, the anisotropy of the crystal is reflected by different absorption coefficients for the different crystallographic directions. The general tendency that the absorption is stronger in π polarization than in σ polarization is also observed in many ESA spectra of Er:YLF (see below). Er:KYF exhibits quite broad bands in comparison with the other investigated crystals because there are six different lattice sites for rare-earth ions in the host lattice.[24,25]

B. Fluorescence

The fluorescence spectra of the Er-doped crystals excited with an argon-ion laser at 488 nm wavelength were measured with a S1 photomultiplier attached to a 0.5 m spectrometer. The lock-in technique yielded an improved signal-to-noise ratio.

Since the $^4S_{3/2} \rightarrow {}^4I_{15/2}$ laser transition is a ground-state transition, the emission cross sections in principle can be calculated from the ground-state absorption cross sections by the reciprocity method under the condition that the absorption and emission cross sections on a single Stark level transition are the same.[26] Differences in the measured effective cross sections of a specific transition in absorption and emission might then only occur due to different Boltzmann populations of the considered starting levels. This assumption might be violated by vibronic interactions, but the deviation

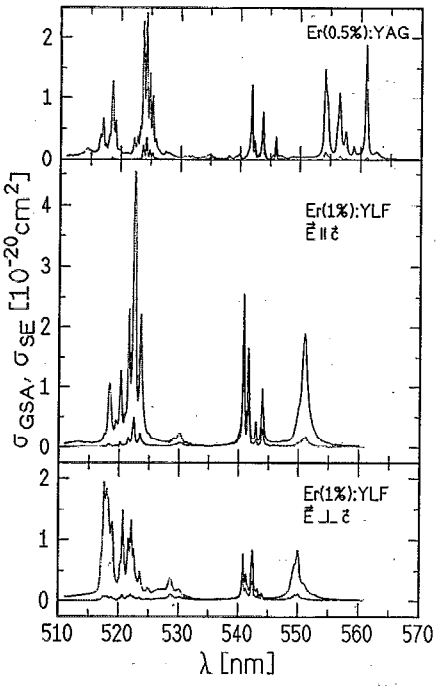

FIG. 3. Emission (solid line) and ground-state absorption (broken line) cross sections of Er:YAG and Er:YLF.

of about 20% for the determination of emission cross sections (measured in the case of Nd:YAG[27]) is acceptable for the purpose of this work.

Since the focal point of this work is the $^4S_{3/2} \rightarrow {}^4I_{15/2}$ laser transition, the spectra of the emission cross sections obtained from the fluorescence spectra of Er(0.5%):YAG and Er(1%):YLF as examples for an oxide and a fluoride crystal are shown from the green to yellow spectral range (Fig. 3). A comparison of absorption and emission cross sections shows that the transitions at 561 nm (Er:YAG) and 551 nm (Er:YLF, $\mathbf{E} \| \mathbf{c}$) are the most probable laser transitions with respect to the ground-state absorption. The ground-state absorption and emission cross sections at the laser wavelengths of Er:YAG and Er:YLF obtained from these spectra are summarized in Table I.

C. Excited-state absorption and stimulated emission

The ESA and stimulated emission (SE) measurements were performed with a pump and probe technique. Two different setups were used to measure the temporal behavior of the excited-state absorption and stimulated emission spectra as well as the stationary spectra.

TABLE I. Stimulated emission and ground-state absorption cross sections of Er-doped YAG and YLF on the $^4S_{3/2} \rightarrow {}^4I_{15/2}$ laser transition.

Crystal	λ (nm)	σ_{SE} (10^{-20} cm^2)	σ_{GSA} (10^{-20} cm^2)
Er:YAG	561	1.8	0.05
Er:YLF	551	1.9 ($\mathbf{E} \| \mathbf{c}$), 0.3 ($\mathbf{E} \perp \mathbf{c}$)	0.2 ($\mathbf{E} \| \mathbf{c}$), 0.04 ($\mathbf{E} \perp \mathbf{c}$)

1. Time-resolved measurement of excited-state absorption and stimulated emission

The fundamental setup for the time-resolved ESA and SE measurements is described in detail elsewhere.[28,29] The basic scheme is the following. The investigated crystal is excited with an excimer laser pumped dye laser (pump beam). The probe beam generated by a Xe flashlamp is recorded with and without excitation of the crystal by an optical multichannel analyzer attached to a 0.25 m spectrometer. Furthermore, spontaneous emission and scattering of the pump beam are corrected for by additional measurements without the probe beam. The time-resolved measurements of the ESA and SE spectra were performed by electronically adjusting the delay Δt between pump and probe beam. According to Lambert–Beer's law, an incident light intensity I_0 at a specific wavelength λ yields a transmitted intensity

$$I_u = I_0 e^{-\sigma_{GSA} n_0 d} \tag{1}$$

for the unpumped crystal and

$$I_p = I_0 \exp\left(-\left(\sigma_{GSA}(n_0 - n_e) + \sum_i \left[(\sigma_{ESA,i} - \sigma_{SE,i}) n_i\right]\right) d\right) \tag{2}$$

for the pumped crystal. Here σ_{GSA} is the ground-state absorption cross section, $\sigma_{ESA,i}$ and $\sigma_{SE,i}$ are the cross sections of the excited-state absorption and the stimulated emission originating from the different excited levels indicated with i. Furthermore, n_0 is the doping concentration, n_i the population density of the excited state i, and n_e the total excitation density given by

$$n_e = \sum_i n_i . \tag{3}$$

Except for n_0, all these densities depend on the delay time between pump and probe beam. Equations (1)–(3) yield the following expression:

$$\sum_i \left(\frac{n_i}{n_e}(\sigma_{ESA,i} - \sigma_{SE,i})\right) = \sigma_{GSA} + \frac{1}{n_e d} \ln \frac{I_u}{I_p} . \tag{4}$$

The quantity $\ln(I_u/I_p)$ is given by the measurements of I_u and I_p. If there are regions in the $\ln(I_u/I_p)$ spectrum where neither ESA nor SE but bleaching of the ground-state absorption occurs, the total excitation density n_e can accurately be determined by

$$n_e = -\frac{1}{\sigma_{GSA} d} \ln \frac{I_u}{I_p} \tag{5}$$

because the left-hand side of Eq. (4) is equal to zero in this case. Then this excitation density n_e and Eq. (4) yield the difference of ESA and SE for the whole spectral range, weighted by the relative excitation densities n_i/n_e and summarized over all possible transitions at the considered wavelength originating from an excited state. The time-resolved measurements of these effective cross sections can be used to

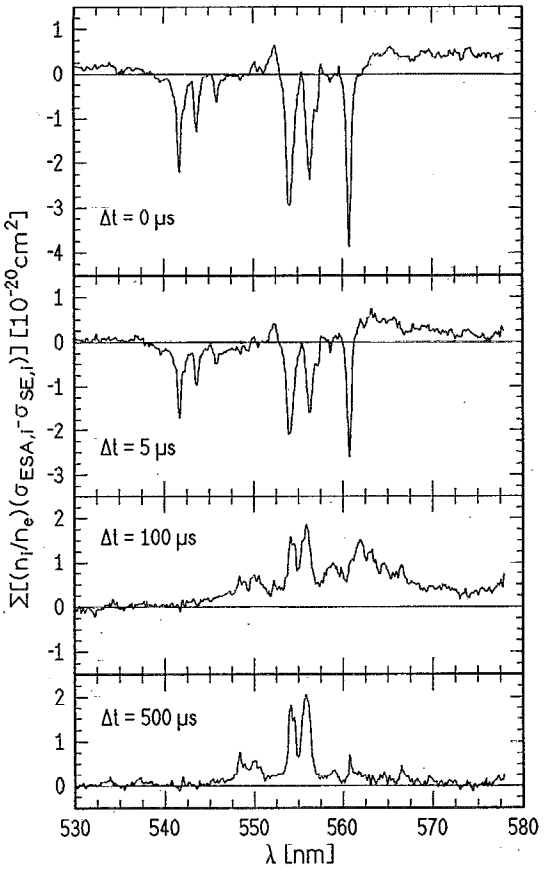

FIG. 4. Time-resolved ESA and SE spectra of Er(1%):YAG in the green to orange spectral range.

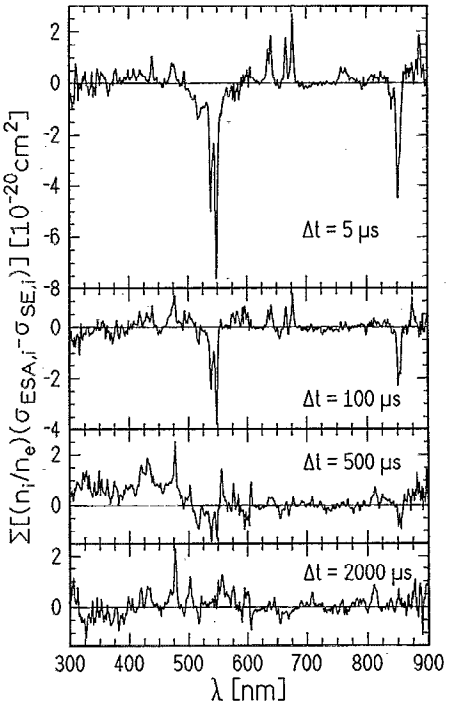

FIG. 5. Time-resolved ESA and SE spectra of Er(1%):YLF for E‖c.

determine the cross sections of ESA and SE for the whole investigated spectral range as well as the population densities of the excited states.[23]

The temporal behavior of the ESA and SE of Er(1%):YAG is shown in Fig. 4 with a resolution of about 0.4 nm. After excitation at 487.6 nm into the $^4F_{7/2}$ level, the Er^{3+} ions rapidly (<1 μs) relax into the upper laser level $^4S_{3/2}$ by phonon emission. For short delay times between pump and probe beam, the stimulated emission $^4S_{3/2} \rightarrow {}^4I_{15/2}$ between 540 and 565 nm with effective cross sections of the order of 10^{-20} cm^2 dominates the spectrum.

Due to the short lifetime of the $^4S_{3/2}$ level [15.9 μs (Ref. 30)], the lower metastable levels $^4I_{11/2}$ and $^4I_{13/2}$ are rapidly populated, whereas the population of other excited states can be neglected here because of their short lifetimes. Therefore, after a delay time of 100 μs, ESA originating from the metastable levels $^4I_{11/2}$ and $^4I_{13/2}$ is observed. The longer lifetime of the $^4I_{13/2}$ (7.6 ms) in comparison with the $^4I_{11/2}$ state (99 μs) is reflected by the fact that after a delay time of 500 μs, ESA starting from the $^4I_{13/2}$ is dominating. In the green and yellow spectral range shown in Fig. 4, the ESA is attributed to the $^4I_{13/2} \rightarrow {}^2H_{9/2}$ transition in this case. ESA transitions originating from both metastable levels $^4I_{11/2}$ and $^4I_{13/2}$ occur, in particular, close to the laser wavelength of 561 nm, so achieving cw laser action of Er:YAG on the $^4S_{3/2} \rightarrow {}^4I_{15/2}$ transition is expected to be much more difficult than in the pulsed mode. Note that in the cw case, the population densities of the $^4I_{11/2}$ and $^4I_{13/2}$ levels are much higher than that of the $^4S_{3/2}$.

In the case of Er(1%):YLF, the ESA and SE spectrum was measured between 300 and 900 nm (Figs. 5 and 6). The resolution of these spectra was about 4 nm. Again, the upper laser level $^4S_{3/2}$ was populated via excitation of the short living $^4F_{7/2}$ level (τ<1 μs) at 486 nm, so for a delay time between the pump and probe beam of 5 μs, the $^4S_{3/2}$ level with a lifetime of 400 μs (Ref. 31) is populated almost exclusively ($n_i/n_e \approx 1$) and ESA and SE transitions starting from this level are observed only. These transitions decrease with increasing delay times according to the lifetime of the $^4S_{3/2}$ level. The increasing population of the metastable $^4I_{11/2}$ and $^4I_{13/2}$ states yields ESA transitions starting from these levels. The branching ratios of the decay of the $^4S_{3/2}$ (Ref. 32) and the lifetimes of the $^4I_{11/2}$ and $^4I_{13/2}$ states (2.9 and 10 ms, respectively[31]) yield comparable population densities of the $^4I_{11/2}$ and $^4I_{13/2}$ states, even for delay times on the order of milliseconds. Therefore, ESA transitions starting from both levels are observed in the spectrum with a delay of 2 ms between the pump and probe beam.

Besides the SE in the green spectral range ($^4S_{3/2} \rightarrow {}^4I_{15/2}$), the spectra with short delay times exhibit stimulated emission on the transition $^4S_{3/2} \rightarrow {}^4I_{13/2}$ around 850 nm. Upconversion laser action on this transition in Er:YLF has already been demonstrated at 851 nm wavelength.[33] For a delay of 2 ms, ESA occurs near 810 nm, which may be used for ESA pumping (see Sec. III C).

In order to investigate the influence of ESA on the laser transition at 551 nm (see Sec. III), the spectra of ESA and SE were measured with a higher resolution (0.4 nm) in this spectral range (Figs. 7,8). The emission cross section of Er:YLF

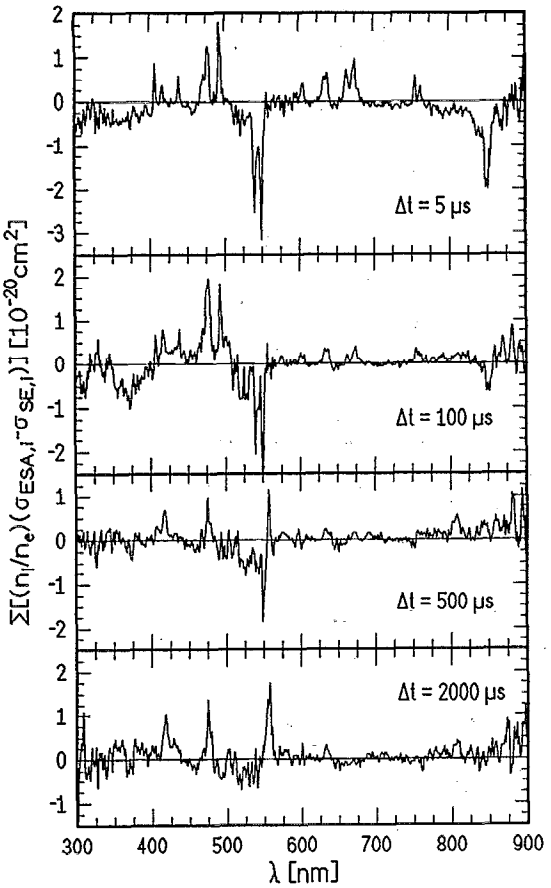

FIG. 6. Time-resolved ESA and SE spectra of Er(1%):YLF for E⊥c.

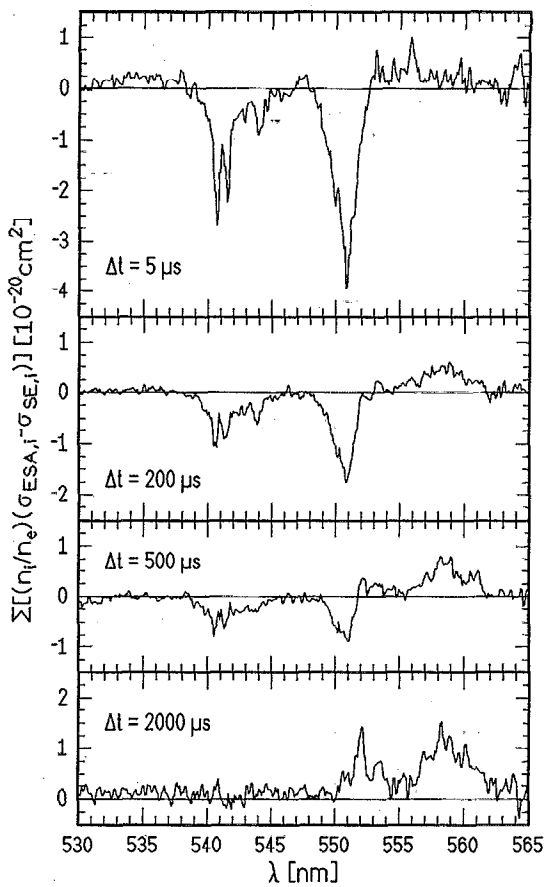

FIG. 7. Time-resolved ESA and SE spectra of Er(1%):YLF for E∥c.

at 551 nm is for **E∥c** more than two times higher than for **E⊥c**. It is obvious that ESA occurs in the considered spectral region for long delay times after the excitation, but in contrast to Er:YAG, the influence on the laser at 551 nm is very small. The upper limit of the effective ESA cross section 2 ms after excitation is on the order of some 10^{-21} cm^2. This is confirmed by the cw ESA measurements (Sec. II C 2) and the quasi-cw laser oscillation in Er:YLF (Sec. III B).

2. Measurement of excited-state absorption with continuous-wave excitation

In order to investigate the influence of ESA on the ${}^4S_{3/2} \rightarrow {}^4I_{15/2}$ laser transition in the green spectral range in more detail and to investigate the possibilities of cw upconversion pumping of the ${}^4S_{3/2}$ level at 810 and 970 nm, ESA measurements under cw excitation were performed with a pump and probe technique in a setup that has already been used for investigations on Ni^{2+}-doped crystals.[34,35] The transmitted probe beam of a halogen lamp is analyzed with a 0.5 m spectrometer, which allows measurements with a higher spectral resolution than in the setup for pulsed excitation. A good signal-to-noise ratio is achieved by a double modulation scheme of pump and probe beam, which is described elsewhere.[36,37] In this setup the small change $\Delta I = I_p - I_u$ is measured directly. This is done by chopping the pump beam of a krypton ion laser and recording the resulting modulation of the probe beam intensity with a lock-in amplifier. The spectra are then evaluated with the relationship

$$-\ln\left(\frac{I_u}{I_p}\right) = \ln\left(1+\frac{I_p - I_u}{I_u}\right) = \ln\left(1+\frac{\Delta I}{I_u}\right). \tag{6}$$

Since the variation of the probe beam intensity due to ESA or SE is usually on the order of a few percents or less, the approximation

$$-\ln\left(\frac{I_u}{I_p}\right) \approx \frac{(I_p - I_u)}{I_u} = \frac{\Delta I}{I_u} \tag{7}$$

can be made. The spectra can be calibrated for absolute cross sections in the same way as described in Sec. II C 1 with the bleaching of the GSA bands.

For a sufficient excitation density, many of the cw measurements were performed with crystals with a higher Er concentration than in the laser experiments because the absorption at the pumping wavelength is rather low. The results are shown in Fig. 9 for the green and yellow spectral range.

In the case of Er(2%):YAG, ESA occurs at the laser wavelength of 561 nm due to the transition ${}^4I_{13/2} \rightarrow {}^2H_{9/2}$, which would reduce the efficiency of potential cw laser operation of this material. This result is also confirmed by the time-resolved ESA measurements (Fig. 4). Due to the shorter

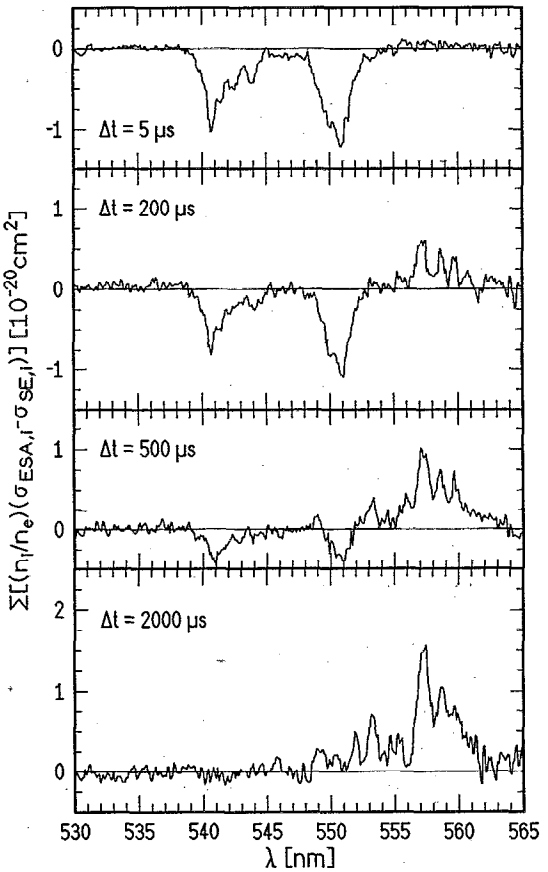

FIG. 8. Time-resolved ESA and SE spectra of Er(1%):YLF for $\mathbf{E} \perp \mathbf{c}$.

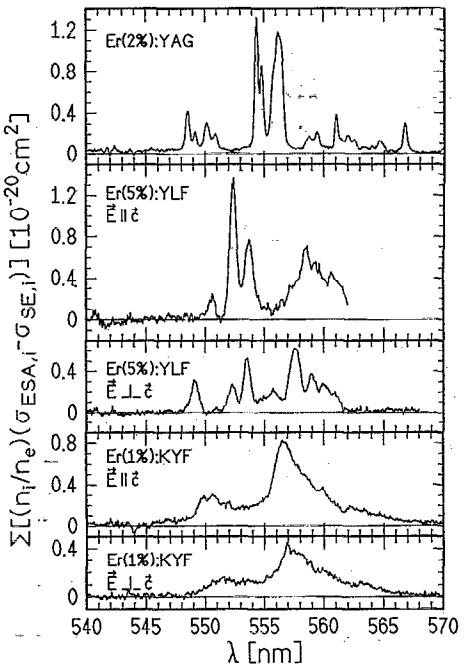

FIG. 9. Continuous-wave ESA spectrum of Er(2%):YAG (resolution: 0.2 nm), Er(5%):YLF (resolution: 1.6 nm), and Er(1%):KYF (resolution: 1.6 nm).

lifetimes of the $^4S_{3/2}$ and $^4I_{11/2}$ states in comparison with the $^4I_{13/2}$ state (see Sec. II C 1), transitions originating from the $^4I_{13/2}$ level dominate the cw ESA spectrum.

The pulsed ESA measurements on Er:YLF did not allow an accurate determination of the influence of ESA on the laser transition at 551 nm wavelength (Sec. II C 1). The cw measurement shows that in this material, the ESA cross section at the lasing wavelength is very small and that ESA should not influence the laser properties significantly. Due to the bigger linewidths of Er:YLF in comparison to Er:YAG, a resolution of the Er:YLF spectra of 1.6 nm was sufficient. The cw ESA spectrum of Er(5%):YLF contains transitions starting from both the $^4I_{11/2}$ and the $^4I_{13/2}$ multiplet because these levels have comparable lifetimes (2.9 and 10 ms, respectively[31]).

Continuous-wave ESA of Er(1%):KYF in the green and yellow spectral range was also investigated. The quite broad ESA bands in this spectral range, which are also shown in Fig. 9 (experimental resolution: 1.6 nm), affect the $^4S_{3/2} \rightarrow {}^4I_{15/2}$ laser transition in this material. Therefore, it might be difficult to achieve cw laser emission of this material at 562 nm wavelength.

3. ESA pumping

Green solid-state lasers are of special interest, in particular if it is possible to pump them with laser diodes in order to realize very compact laser systems. Up to now powerful laser diodes are available for the dark red and infrared spectral range only, especially around 810 and 970 nm. Er^{3+} exhibits both ground-state and excited-state absorption in this spectral range, so these transitions are interesting for upconversion pumping (in the sense that the energy of the pump photons is less than the energy of the green laser photons). Therefore, the ESA of Er-doped crystals was also investigated in this spectral range (Fig. 10). Due to the spectral sensitivity of the optical multichannel analyzer, no time-resolved measurements could be performed in the spectral range near 970 nm (compare Figs. 5 and 6).

Since the lifetimes of the $^4S_{3/2}$ and the $^4I_{11/2}$ states are much shorter than that of the $^4I_{13/2}$ in the case of Er:YAG (see Sec. II C 1), practically only transitions originating from the $^4I_{13/2}$ state are observed in the cw ESA spectrum, in particular around 800 nm. The corresponding ESA cross sections are on the order of 10^{-21} cm^2. Note that at 970 nm no ESA peaks are present, although from the energy-level diagram ESA transitions starting from the $^4I_{11/2}$ state are expected in this wavelength region. This confirms that the population of the $^4I_{11/2}$ level is very low.

In contrast, the cw ESA spectra of Er(5%):YLF, also shown in Fig. 10, exhibit not only transitions originating from the $^4I_{13/2}$, but also from the $^4I_{11/2}$ state because both levels are populated. Therefore, the ESA transitions $^4I_{11/2} \rightarrow {}^4F_{7/2}$ around 970 nm with maximum effective cross sections (i.e., $(n_i/n_e) \times \sigma_{\mathrm{ESA},i}$) on the order of 10^{-20} cm^2 ($\mathbf{E} \| \mathbf{c}$) are observed in this spectrum. The π component of this transition is again much stronger than the σ component.

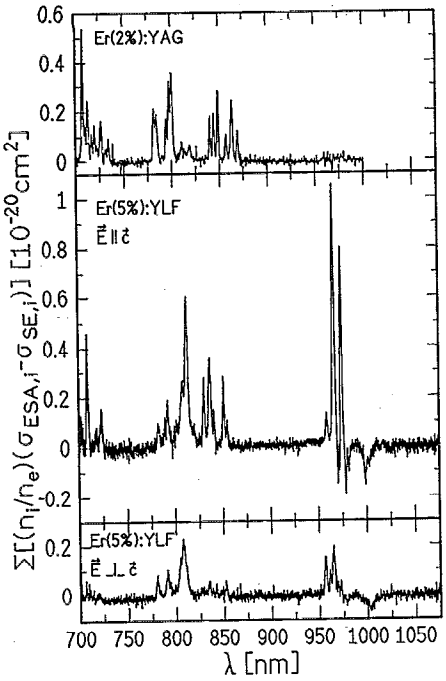

FIG. 10. Continuous-wave ESA spectrum of Er(2%):YAG and Er(5%):YLF in the dark red and infrared spectral range (resolution: 1.6 nm).

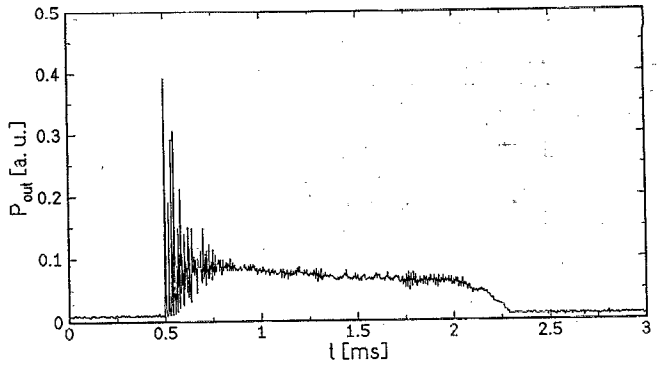

FIG. 11. Temporal behavior of the output power of the quasi-cw Er(1%):YLF laser at 551 nm wavelength.

III. LASER EXPERIMENTS

In all the laser experiments discussed below a nearly concentric resonator with $r=5$ cm and tight focusing of the pump radiation ($f=5$ cm) was used in order to obtain low laser thresholds.

A. Direct excitation with short pulses

According to the time-resolved ESA measurements, pulsed green room-temperature laser emission should be possible in all crystals that were investigated (Sec. II C). This was proved for Er(1%):YLF and Er(1%):YAG as well as for Er(1%):$Lu_3Al_5O_{12}$ (LAG) crystals which were excited in the blue spectral range by an excimer laser pumped dye laser with a pulse width of about 50 ns.[20] The pulse duration was short compared to the upper laser level lifetime in all investigated samples [e.g., 15.9 μs in Er(1%):YAG (Ref. 30)]. The best results were obtained with a 2.4 mm long Er(1%):YLF sample pumped at 486 nm wavelength. With an output coupling of 2%, a slope efficiency of 6% and a maximum output energy of about 30 μJ at 551 nm at an absorbed pump energy of 570 μJ were obtained. As expected from the fluorescence and ESA measurements (Figs. 3, 5–8), laser oscillation occurred in π polarization. With the observed pulse width of about 50 ns, the maximum output energy corresponded to a peak power of 600 W. These results can probably be further improved by optimizing output coupling, crystal length, and mode matching. In contrast to Er:YLF, laser oscillation at 561 nm in the garnets ceased after a few shots in Er:YAG and after about half an hour in Er:LAG (repetition rate 1 Hz). The output energy of these lasers was very much lower than that of Er:YLF. However, the thresholds of the Er-doped garnets were lower than that of Er:YLF because of smaller reabsorption losses at the laser wavelength. The reason for the poor laser performance of the Er-doped garnets is not yet fully understood. Perhaps stationary color centers are created in these garnets.

Laser oscillation could not be achieved in Er(1.5%):$YAlO_3$ with this setup although stimulated emission on the $^4S_{3/2}\rightarrow{}^4I_{15/2}$ transition has been measured.[23] The reason for that is, up to now, not clear. The Er(1%):KYF sample has not yet been studied systematically with this setup.

B. Direct excitation by a quasi-cw pump laser

In this experiment the Er(1%):YLF crystal was excited "all lines" by an argon-ion laser with a duty cycle of 1:10. Under quasi-cw excitation, mainly the metastable $^4I_{11/2}$ and $^4I_{13/2}$ levels are populated and only a small fraction of the excited Er ions remains in the $^4S_{3/2}$ upper laser level because of its shorter lifetime. Therefore, laser oscillation is more difficult to obtain in this case. Note that these populations are used in a two-step upconversion pumping scheme (see below). With mirrors highly reflecting at the laser wavelength, the laser reached threshold at a quasi-cw absorbed pump power of 0.8 W. The time evolution of the output power is shown in Fig. 11. The average output power at 551 nm was 20 μW. Although the laser emits significantly longer (>1.5 ms) than the upper laser level lifetime (0.4 ms), cw operation could not be achieved. This was probably due to the insufficient cooling of the crystal.

Under quasi-cw pumping the populations of the metastable $^4I_{11/2}$ and $^4I_{13/2}$ levels are higher than that of the upper laser level. As laser oscillation with π polarization can be achieved under these conditions, π polarized parasitic ESA from the metastable levels must be very low at the laser wavelength in the case of Er(1%):YLF. This result is in good agreement with the ESA measurements (Sec. II C; Figs. 5, 7, and 9).

C. Upconversion pumping

In crystals with a high Er concentration (more than about 5%), the upper laser level $^4S_{3/2}$ is efficiently depopulated at ambient temperature. The $^4S_{3/2}$ is thermally coupled with the $^2H_{11/2}$, which is depopulated by the cross relaxation $^2H_{11/2}$,

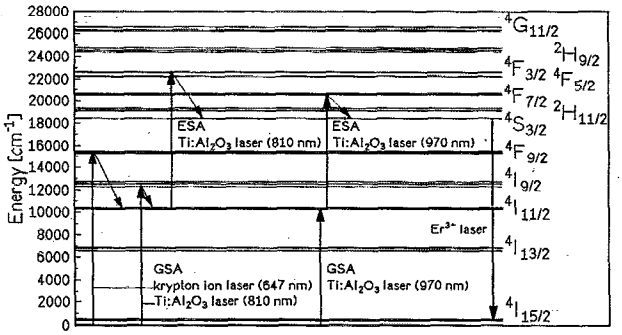

FIG. 12. Pumping schemes for Er-doped upconversion lasers.

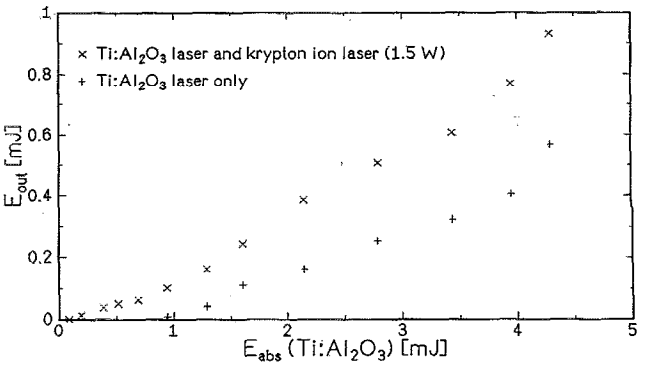

FIG. 13. Input-output diagram for the Er(1%):YLF upconversion laser at 551 nm wavelength.

$^4I_{15/2} \rightarrow {}^4I_{9/2}$, $^4I_{13/2}$. The upper Stark levels of the ground state are significantly thermally populated in many cases, too. Therefore, at high Er concentrations one often encounters high reabsorption losses at the laser wavelength. At low (about 1%) Er concentrations both of these difficulties are reduced. Unfortunately, at low concentrations the "true" upconversion processes (e.g., $^4I_{11/2}$, $^4I_{11/2} \rightarrow {}^4F_{7/2}$, $^4I_{15/2}$) are inefficient (as is the cross relaxation). Consequently, the upper laser level was populated via a two-step process involving GSA and ESA. From the ESA measurements (Sec. II C; Figs. 5 and 10) it can be seen that in such a scheme the laser can be pumped efficiently either near 810 nm or near 970 nm. With respect to future diode pumping of these lasers, it should be noted that high power laser diodes are available at these wavelengths.

1. Excitation near 810 nm

As the output energy of the flashlamp pumped Ti:sapphire laser used for the first experiment was low near 970 nm, the crystals were excited near 810 nm with this setup.[21] However, the GSA of the investigated crystals near 810 nm is very weak. Therefore, the crystals were additionally pumped by a krypton ion laser at 647 nm wavelength, which matches the GSA into the $^4F_{9/2}$ level in many crystals. The complete pumping scheme is shown in Fig. 12 together with that using a pump wavelength of 970 nm (see below). Of course, in principle, an additional pump channel due to a relaxation into the metastable level $^4I_{13/2}$ followed by the ESA transition $^4I_{13/2} \rightarrow {}^2H_{11/2}$ and a nonradiative decay into the upper laser level $^4S_{3/2}$ cannot be excluded right from the beginning. Therefore, in the case of Er:YLF the pump process was investigated in detail (see Sec. III C 2).

The flashlamp pumped Ti:sapphire laser had a pulse width of 50 μs and an emission bandwidth of about 5 nm, which is comparable to that of a high power laser diode. The best results were again obtained with Er(1%):YLF. The output energy of the 6.9 mm long crystal is shown in Fig. 13.

With both pump lasers a maximum output energy of 0.93 mJ at 551 nm wavelength has been achieved. Pumping with only the Ti:sapphire laser yielded a slope efficiency of about 15% and a maximum output energy of 0.57 mJ. In spite of an output coupling of more than 75% through each mirror, simultaneous laser oscillation at 850 nm on the $^4S_{3/2} \rightarrow {}^4I_{13/2}$ transition has been observed in Er(1%):YLF. Suppression of this laser transition may further increase the efficiency of the green laser transition because both transitions originate from the same upper laser level. On the other hand, with suitable mirrors it should be easy to realize a diode pumped laser at 850 nm wavelength.

With this setup laser oscillation could also be demonstrated in Er(1%):KYF with a somewhat lower output energy: 139 μJ with both the krypton ion laser and the Ti:sapphire laser as pump sources and 38 μJ when pumping with the Ti:sapphire laser only. The laser emission at 562 nm wavelength was π polarized. In Er(0.5%):YAG the output energy decreased after the first few shots and then stabilized. However, this output energy was orders of magnitude lower than that of the fluorides. Again, in Er(1.5%):$YAlO_3$ laser oscillation could not be achieved. Here it should be noted that the match of the emission of the krypton ion laser at 647 nm and the absorption spectrum of Er:$YAlO_3$ is very poor.

Recently, green upconversion cw laser action of Er:YLF at room temperature was reported, too.[22] The crystal was pumped at 810 nm, which is the same wavelength as that used in the pulsed experiments described before. This clearly confirms that ESA losses at 551 nm are at least very small.

2. Pumping mechanism in the case of Er(1%):YLF

It was already claimed that a two-step process consisting of a GSA and an ESA process (see Fig. 12) is the dominant mechanism populating the upper laser level in the case of Er(1%):YLF. This assumption is supported by additional measurements. First of all, the dependence of the green output energy on the wavelength of the Ti:sapphire laser was measured with and without additional krypton ion laser pumping. For that purpose, the emission bandwidth of the Ti:sapphire laser was reduced to less than 1 nm by a third element in the birefringent filter. The result is shown together with the ESA and GSA spectra of Er:YLF in Fig. 14.

As expected, the output energy correlates with both GSA and ESA. In case of a "true" upconversion process ($^4I_{11/2}$, $^4I_{11/2} \rightarrow {}^4I_{15/2}$, $^4F_{7/2}$) the output energy would be correlated with the GSA only. Considering the energy levels of Er:YLF,[13,38] it should be noted that besides the ESA transitions $^4I_{11/2} \rightarrow {}^4F_{3/2}$ around 810 nm and $^4I_{11/2} \rightarrow {}^4F_{5/2}$ (~830–840 nm), the transitions $^4I_{13/2} \rightarrow {}^2H_{11/2}$ and

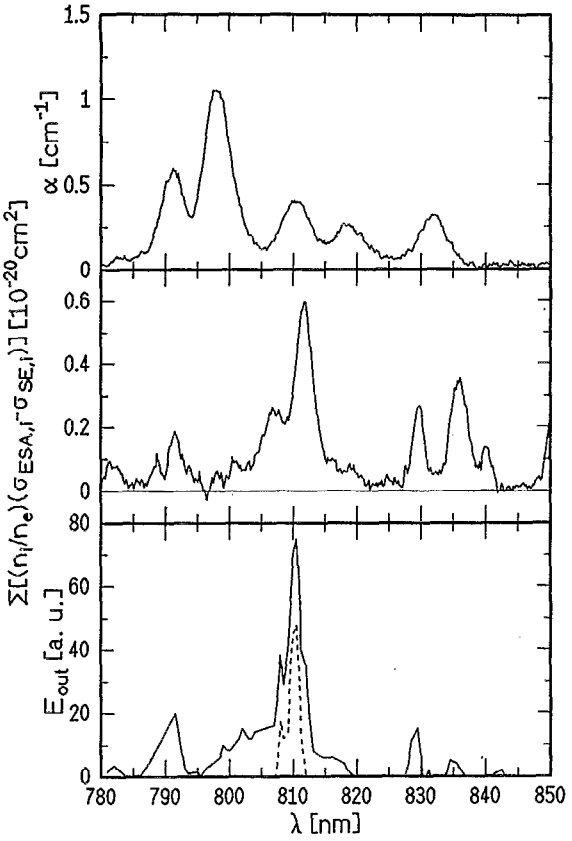

FIG. 14. π-polarized GSA and ESA spectra of Er(5%):YLF as well as output energy of the Er(1%):YLF laser at 551 nm in dependence of the pump wavelength when pumping with both the krypton ion laser at 647 nm wavelength and the Ti:sapphire laser (solid line) and with the Ti:sapphire laser only (broken line).

$^4I_{13/2} \rightarrow {}^4S_{3/2}$ (~780–805 nm and 835–855 nm, respectively) may also be used for pumping the upper laser level $^4S_{3/2}$.

In addition, time-resolved fluorescence measurements were carried out. When laser oscillation took place, the spontaneous fluorescence at 850 nm originating from the upper laser level $^4S_{3/2}$ and at 970 nm originating from the $^4I_{11/2}$ level were detected transversally to the resonator axis. These fluorescence signals are proportional to the populations of the corresponding levels. The results are shown in Figs. 15 and 16. It can be seen that the upper laser level is immediately populated during the pump pulse of the Ti:sapphire laser as expected for the ESA process. In case of the true upconversion process ($^4I_{11/2}, {}^4I_{11/2} \rightarrow {}^4I_{15/2}, {}^4F_{7/2}$) the upper laser level would be populated with a rate proportional to the square of the population of the $^4I_{11/2}$ level. However, the population of the $^4I_{11/2}$ reaches its maximum at about 0.5 ms after the Ti:sapphire pump pulse (Fig. 16). At this time the population of the upper laser level already decays significantly. Finally, the green laser emission terminates together with the Ti:sapphire laser pulse as expected for the ESA process.

3. Excitation near 970 nm

Using a more powerful Ti:sapphire laser at the Festkörperlaserinstitut in Berlin, it was possible to excite the crystals

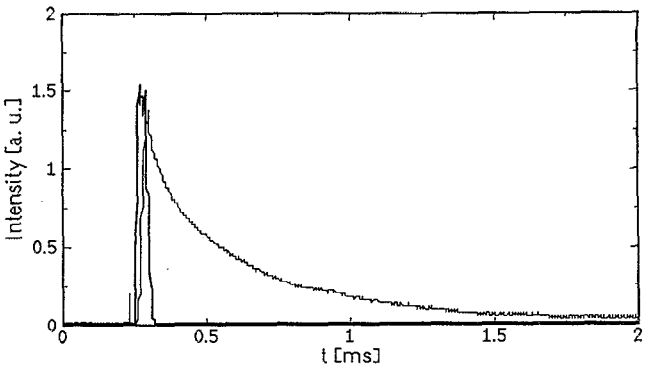

FIG. 15. Ti:sapphire pump pulse (fat line) and fluorescence at 850 nm wavelength originating from the $^4S_{3/2}$ level when pumping with the krypton ion laser at 647 nm and the Ti:sapphire laser at 810 nm.

near 970 nm, where higher GSA and ESA cross sections were measured (see Figs. 2 and 10). In this case no additional pump source was used. The pumping scheme is shown in Fig. 12. The upper laser level $^4S_{3/2}$ is populated by GSA into the $^4I_{11/2}$ state and ESA on the $^4I_{11/2} \rightarrow {}^4F_{7/2}$ transition, followed by a nonradiative decay into the upper laser level.

The pulse width of the Ti:sapphire laser in this experiment was only 4 μs. Its emission bandwidth was again on the order of 5 nm. Tuning of this laser was achieved by three intracavity prisms.

The output energy of the 6.9 mm long Er(1%): YLF crystal is shown in Fig. 17. With a pulse width of 4 μs, the maximum output energy of 0.9 mJ corresponded to a peak power of 225 W. In spite of the smaller pump photon energy, in this case the slope efficiency of almost 14% is lower than that under excitation near 810 nm. This is probably caused by the worse spectral overlap of GSA and ESA around 970 nm when compared to 810 nm.

IV. CONCLUSIONS

In this work the spectroscopic parameters of Er-doped YAG, YLF, and KYF were investigated. Excited-state absorption originating from the metastable levels $^4I_{11/2}$ and $^4I_{13/2}$ was shown to affect the green $^4S_{3/2} \rightarrow {}^4I_{15/2}$ laser tran-

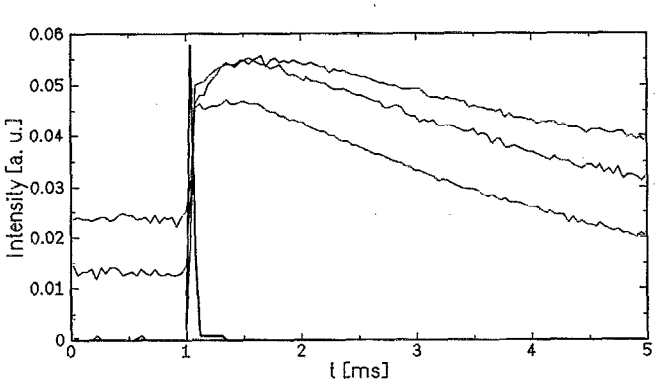

FIG. 16. Ti:sapphire pump pulse (fat line) and fluorescence at 970 nm wavelength originating from the $^4I_{11/2}$ level when pumping with the Ti:sapphire laser at 810 nm for three different pump powers of the krypton ion laser (0, 0.5, and 1 W, bottom to top).

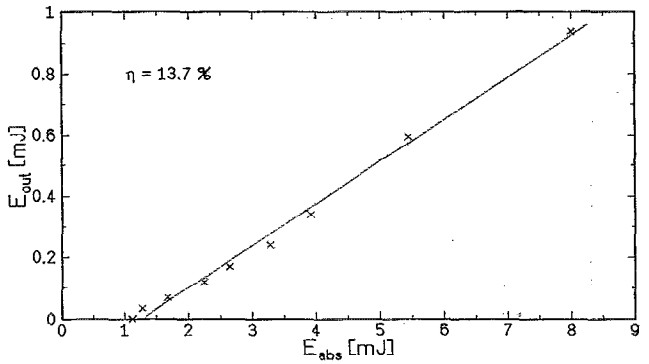

FIG. 17. Input-output diagram for the Er(1%):YLF upconversion laser at 551 nm when pumping at 970 nm wavelength.

sition in the case of Er:YAG and Er:KYF. In the case of Er:YLF, the influence of ESA on the laser transition is only small. This was also confirmed by quasi-cw laser action on this transition when pumping with a chopped argon-ion laser. Stimulated emission at the laser wavelength was measured for Er:YAG and Er:YLF directly after pulsed excitation into the $^4F_{7/2}$, followed by a fast nonradiative decay into the $^4S_{3/2}$ level.

Excited-state absorption was measured around 810 and 970 nm because a combination of these transitions and GSA at the same wavelength can be used for so-called upconversion lasers. Room-temperature upconversion laser action on the green transition $^4S_{3/2} \rightarrow {}^4I_{15/2}$ was realized in Er-doped YLF, KYF, and YAG. In the case of Er:YLF, the pump mechanism could be identified by measurements of ESA and time-resolved fluorescence for pumping at 810 nm wavelength. Pumping the Er:YLF crystal with a Ti:sapphire laser at 810 nm wavelength only, the maximum output energy at 551 nm was 0.57 mJ with a slope efficiency of about 15%. When pumping at 970 nm wavelength, an output energy of 0.9 mJ was achieved with a slope efficiency of almost 14%.

Further investigations of Er-doped crystals should yield an optimization of the pump process of the green upconversion laser in order to increase the output energy and power in the pulsed and in the cw modes, respectively. It might be possible to achieve diode pumped room-temperature cw upconversion laser emission on the $^4S_{3/2} \rightarrow {}^4I_{15/2}$ transition in Er:YLF.

ACKNOWLEDGMENTS

The authors are indebted to G. Phillipps and A. Hoffstädt of the Festkörperlaserinstitut in Berlin who placed the Ti:sapphire laser for the upconversion laser experiments at a pump wavelength of 970 nm at our disposal.

[1] M. A. Haase, J. Qiu, J. M. DePuydt, and H. Cheng, Appl. Phys. Lett. **59**, 1272 (1991).
[2] H. Jeon, J. Ding. W. Patterson, A. V. Nurmikko, W. Xie, D. C. Grillo, M. Kobayashi, and R. L. Gunshor, Appl. Phys. Lett. **59**, 3619 (1991).
[3] L. Goldberg and M. K. Chun, Appl. Phys. Lett. **55**, 218 (1989).
[4] A. Feisst and P. Koidl, Appl. Phys. Lett. **47**, 1125 (1985).
[5] L. F. Johnson and H. J. Guggenheim, Appl. Phys. Lett. **19**, 44 (1971).
[6] J. Y. Allain, M. Monerie, and H. Poignant, Electron. Lett. **26**, 166 (1990).
[7] J. Y. Allain, M. Monerie, and H. Poignant, Electron. Lett. **26**, 261 (1990).
[8] M. Oka and S. Kubota, Jpn. J. Appl. Phys. **31**, 2B 513 (1992).
[9] Y. Kitaoka, S. Ohmori, K. Yamamoto, M. Kato, and T. Sasaki, Appl. Phys. Lett. **63**, 299 (1993).
[10] D. C. Nguyen, G. E. Faulkner, M. E. Weber, and M. Dulick, SPIE **1223**, 54 (1990).
[11] R. J. Thrash and L. F. Johnson, Compact Blue-Green Lasers, Technical Digest Series Vol. 6, paper ThB3 (1992) (unpublished).
[12] T. J. Whitley, C. A. Millar, R. Wyatt, M. C. Brierly, and D. Szebesta, Electron. Lett. **27**, 1785 (1991).
[13] A. A. Kaminskii, *Laser Crystals. Their Physics and Properties*, 2nd ed., Springer Series in Optical Sciences, Vol. 14 (Springer, Berlin, 1990), p. 143.
[14] L. F. Johnson and H. J. Guggenheim, Appl. Phys. Lett. **20**, 474 (1972).
[15] A. J. Silversmith, W. Lenth, and R. M. Macfarlane, J. Opt. Soc. Am. A **3**, P128 (1986).
[16] A. J. Silversmith, W. Lenth, and R. M. Macfarlane, Appl. Phys. Lett. **51**, 1977 (1987).
[17] T. Hebert, R. Wannemacher, W. Lenth, and R. M. Macfarlane, Appl. Phys. Lett. **57**, 1727 (1990).
[18] P. Xie and S. C. Rand, Opt. Lett. **17**, 1198 (1992).
[19] R. R. Stephens and R. A. Mcfarlane, Opt. Lett. **18**, 34 (1993).
[20] R. Brede, T. Danger, E. Heumann, G. Huber, and B. Chai, Appl. Phys. Lett. **63**, 729 (1993).
[21] R. Brede, E. Heumann, J. Koetke, T. Danger, G. Huber, and B. Chai, Appl. Phys. Lett. **63**, 2030 (1993).
[22] F. Heine, E. Heumann, T. Danger, T. Schweizer, G. Huber and B. Chai, Advanced Solid-State Lasers Topical Meeting, Salt Lake City, UT, Postdeadline paper PD5 (1994) (unpublished).
[23] M. Pollnau, E. Heumann, and G. Huber, Appl. Phys. A **54**, 404 (1992).
[24] B. Y. Le Fur, N. M. Khaidukov, and S. Aléonard, Acta Crystallogr. C **48**, 978 (1992).
[25] H. Weidner, P. L. Summers, R. E. Peale, X. X. Zhang, and B. H. T. Chai, Technical Digest of the 1993 International Conference on Luminescence, Storrs, Connecticut, paper M4-39 (1993) (unpublished).
[26] S. A. Payne, L. L. Chase, L. K. Smith, W. L. Kway, and W. F. Krupke, IEEE J. Quantum Electron. **28**, 2619 (1992).
[27] B. F. Aull and H. P. Jenssen, IEEE J. Quantum Electron. **18**, 925 (1982).
[28] H. Stange, Dissertation, Universität Hamburg, 1991.
[29] T. Danger, K. Petermann, and G. Huber, Appl. Phys. A **57**, 309 (1993).
[30] R. Gross, Dissertation, Universität Hamburg, 1992.
[31] J. Rubin, A. Brenier, R. Moncorge, and C. Pedrini, J. Lumin. **36**, 39 (1986).
[32] A. M. Tkachuk, A. V. Poletimova, and M. V. Petrov, Opt. Spectrosc. (USSR) **59**, 680 (1985).
[33] S. A. Pollack, D. B. Chang, and M. Birnbaum, Appl. Phys. Lett. **54**, 869 (1989).
[34] J. Koetke, K. Petermann, and G. Huber, J. Lumin. (to be published).
[35] J. Koetke, Dissertation, Universität Hamburg (to be published).
[36] T. Wegner and K. Petermann, Appl. Phys. B **49**, 275 (1989).
[37] S. Zemon, G. Lambert, W. J. Miniscalco, R. W. Davies, B. T. Hall, R. C. Folweiler, T. Wei, L. J. Andrews, and M. P. Singh, SPIE **1373**, 21 (1990).
[38] G. M. Renfro, J. C. Windscheif, W. A. Sibley, and R. F. Belt, J. Lumin. **22**, 51 (1980).